Mixed Velocity-Temperature Measurements in the Turbulent Wake of a Heated Cylinder

by Arpi Berajeklian

Undergraduate Honours Thesis
Supervisor: Professor L. Mydlarski

Department of Mechanical Engineering
McGill University

A thesis submitted to McGill University in partial fulfillment of the requirements of the Undergraduate Honours Program

Abstract

Simultaneous velocity-scalar measurements were made in a wind tunnel to study the mixing of scalars within turbulent flows. The scalar was temperature, which was considered to be passive. The measurements were made in the turbulent wake of a heated cylinder using hot-wire anemometry and cold-wire thermometry.

Mixed velocity-temperature measurements permitted (i) the calculation of the turbulent heat flux, which describes how velocity fluctuations mix the scalar, and (ii) the turbulent Prandtl number distribution. The former includes the transverse profile of the turbulent heat flux and the turbulent heat flux co-spectra (in both the longitudinal and transverse directions). The inertial subrange was studied and a power-law scaling was observed. The turbulent Prandtl number (Pr_T) distribution across the wake was also calculated from the above measurements.

The co-spectra exhibited inertial-range scalings similar to those observed in homogeneous, isotropic turbulence even though the present flow is inhomogeneous. The turbulent Prandtl number distribution, which is generally assumed to be unity in the modeling community, was found to be different from one and varied significantly across the wake.

Résumé

Des mesures simultanées de vitesse et de scalaire sont prises dans une soufflerie pour comprendre le mélange des scalaires en écoulements turbulents. L'écoulement turbulent en question est le sillage d'un cylindre chauffé où la température est un scalaire passif. Les mesures de vitesse sont prises en utilisant l'anémométrie à fil chaud et les mesures de température sont prises en utilisant la thermométrie à fil froid.

Les mesures simultanées de vitesse et de température permettent de calculer i) le flux turbulent du scalaire qui décrit comment les fluctuations de vitesse mélangent le scalaire et ii) la distribution du nombre de Prandtl turbulent. Le premier inclut le profil transversal du flux turbulent ainsi que le cospectre du flux turbulent (longitudinal et transversal). La zone inertielle est examinée, où une loi de puissance a été observée.

La zone inertielle du flux turbulent a démontré un comportement semblable à celui observé en écoulements turbulents homogènes et isotropes. La distribution du nombre de Prandtl turbulent, généralement supposé d'être égale à un dans les simulations numériques du transfert thermique, était différente de un et variait de façon significative à travers le sillage.

Acknowledgements

I would like to thank my supervisor Professor Mydlarski. His enthusiasm for his research has given me motivation to work on my thesis. He has given me great support and advice throughout my research.

I would also like to thank Jason Lepore for his generous help in the lab during my experiments. I have learned a great deal from his experience.

Furthermore, a great thanks is extended to Alexandra Rhéaume for inspiring me to do my research in turbulence.

In addition, Georges Tewfik and Mario Iacobaccio from the measurement lab have given great advice throughout my research when dealing with the electronics of my experimental setup. I appreciate their help.

Finally, I would like to thank the National Sciences and Engineering Research Council for supporting my research during the summer of 2007.

Table of Contents

List of Figures

List of Tables

Nomenclature

A, B, n	Hot-wire calibration constants for isothermal flows
$\overline{A}$, $\overline{B}$, $T_{w,a}$, $T_{w,b}$	Hot-wire calibration constants for non-isothermal flows
C, D	Cold-wire calibration constants
D	Cylinder diameter
E	Output voltage
E_{uu}	Power spectral density of the turbulent kinetic energy
$E_{\theta\theta}$	Power spectral density of the scalar (temperature) variance
$E_{u\theta}$	Longitudinal heat flux co-spectrum
$E_{v\theta}$	Transverse heat flux co-spectrum
f_c	Cut-off frequency of the cold-wire
γ_T	Turbulent thermal diffusivity
h	Half-width of a Gaussian profile
k	Ratio of two cooling modes (cooling by cross- and parallel-flow)
$\Pr_T$	Turbulent Prandtl number
Re_D	Reynolds number $\left(\mathrm{Re}_D = \dfrac{U_\infty D}{\nu}\right)$
ρ_{uv}	Correlation coefficient for variables u and v
σ	Standard deviation
T_∞	Free-stream temperature
$\langle T \rangle$	Mean temperature
$\langle T \rangle - T_\infty$	Mean temperature excess

τ_w	Time constant of the cold-wire
τ_e	Electronics time constant of the constant current anemometer
θ	Scalar (temperature) fluctuation
θ_{eff}	Effective angle of the X-wire
U_∞	Free-stream velocity
U	Instantaneous longitudinal velocity
$< U >$	Mean longitudinal velocity
u	Longitudinal velocity fluctuation
$\frac{U_c}{U_\infty}$	Centreline to free-stream velocity ratio
$< uv >$	Turbulent Reynolds stress
$< u\theta >$	Longitudinal turbulent heat flux
$< v\theta >$	Transverse turbulent heat flux
v	Transverse velocity fluctuation
ν	Kinematic viscosity of air $(15\times10^{-6}\frac{m^2}{s})$
ν_T	Turbulent viscosity
$\frac{\partial < T >}{\partial y}$	Transverse mean temperature gradient
$\frac{\partial < U >}{\partial y}$	Transverse mean velocity gradient

Chapter 1

Introduction

Most flows, whether encountered in nature or in industry, are turbulent. Turbulent flows are remarkable because of their ability to rapidly mix quantities like mass, momentum, and energy. In particular, the mixing of scalars (e.g., temperature, chemical species concentration, etc.) in turbulent flows is common to many applications, including heat transfer, combustion, meteorology, and environmental pollutant dispersion. Therefore, thoroughly understanding the mixing of scalars is necessary to accurately model and predict these phenomena.

Measurements of scalar fields in turbulent flows are common, as are measurements of the velocity field. However, simultaneous measurements of the velocity and scalar fields remain quite rare. That being said, mixed velocity-scalar measurements are essential to understanding the behaviour of scalar fields in turbulent flows because it is the velocity field that predominantly controls the evolution of the scalar field. For example, consider the turbulent scalar flux, which is the scalar analog of the Reynolds stress and is defined as the mean of the product of the scalar and velocity fluctuations. It dictates the behaviour of the mean scalar field in a turbulent flow; consequently, it is of particular interest to scientists and engineers.

1.1 Literature Review

In order to define the objective of this thesis, one must place it in the context of the previous work in the field. Therefore, this section will present a brief overview of the research that motivates the present work.

1.1.1 Turbulence

Turbulence is an important branch of fluid dynamics because the vast majority of flows in engineering applications are turbulent. There are several books and research papers written on the subject of turbulence. Two examples of books pertaining to the study of turbulence are "A First Course in Turbulence" by Tennekes and Lumley (1972) and "Turbulent Flows" by Pope (2000). Turbulence is difficult to define precisely. However, its characteristics are well known; turbulent flows are random, possess large diffusivities, occur at large Reynolds numbers, exhibit three-dimensional vorticity fluctuations, and are dissipative.

As with many engineering subjects, the study of turbulent flows can be performed both experimentally and computationally. Books about experimental studies in turbulence such as "Hot-Wire Anemometry: Principles and Signal Analysis" by Brunn (1995) discuss the measurement techniques used herein. For computational studies, there are three principal techniques used to analyze turbulent flows: Direct Numerical Simulation (DNS) (e.g., Moin and Mahesh, 1998); Large Eddy Simulation (LES) (e.g., Lesieur and Metais, 1996); and Reynolds-Averaged Navier-Stokes simulation (RANS) (e.g., Pope, 2000).

1.1.2 Mixing of Passive Scalars within Turbulent Flows

An interesting aspect of turbulence is the study of passive scalar mixing. As mentioned above, it is common to numerous scientific and engineering phenomena. A *passive* scalar is one that does not disturb the velocity field in which it is injected. Temperature is considered to be a passive scalar when the range of temperature differences is small, rendering buoyancy effects negligible.

A typical example of scalar mixing is the flow within the wake of a heated cylinder. This classic turbulent flow has been studied by many researchers. For example, Fabris (1979) studied conditional sampling in the far wake of a slightly heated cylinder with simultaneous measurements of velocity and temperature. Matsumura and Antonia (1993) studied momentum and heat transport in the intermediate wake of a heated cylinder. They compared the rates at which momentum and heat are transported in the turbulent wake of the cylinder and found that heat is transported more effectively than momentum.

Simultaneous measurements of velocity and temperature are essential to the study of scalar mixing in turbulent flows because only they allow important parameters such as the turbulent scalar flux ($\langle u_i \theta \rangle$) and the turbulent Prandtl number (Pr_T) to be measured. (The turbulent Prandtl number is defined as the ratio of turbulent momentum diffusivity (ν_T) to the turbulent (thermal) diffusivity (γ_T). Alternatively said, it relates how fast turbulence transports momentum compared to energy.)

Theoretically, the "Reynolds analogy" is used to justify the assumption that $\Pr_T$ is equal to unity (Tennekes and Lumley, 1972). Townsend (1976) proposed a qualitative formulation called the rapid distortion hypothesis which explained that the turbulent Prandtl number increases with increasing total strain. Sreenivasan *et al.* (1984) researched the variation of this quantity in shear flows. They gathered experimental results from different researchers and estimated $\Pr_T$ for comparison with the work of Townsend (1976) for different shear flows. This paper concluded that the turbulent Prandtl number, as predicted by Townsend, is underestimated.

Another study of the turbulent Prandtl number is that of Kays (1994) who examined $\Pr_T$ for two different flows: (i) a two-dimensional turbulent boundary layer and (ii) a fully-developed flow in a circular pipe or a flat duct. This paper gathered and analyzed many results from different experiments and computations. Kays made a few conclusions for all regions of these flows. For instance, in the "wake" region (i.e., the external turbulent boundary layer for the first flow and the centerline region for the second flow), $\Pr_T$ is around 0.5-0.7 for moderate and high Prandtl number fluids. He also drew some conclusions on the effect of transpiration, surface roughness, and pressure gradients on the turbulent Prandtl number.

Therefore, although the order of magnitude of the turbulent Prandtl number is unity, studies have shown that the turbulent Prandtl number does vary significantly from one turbulent flow to another, as well as within different turbulent flows.

1.2 Thesis Objectives

The objective of the current research was to obtain a better understanding of passive scalar mixing by studying the relationship between the velocity and scalar fields. This was accomplished by means of simultaneous measurements of (longitudinal and transverse) velocity and temperature. The flow under consideration was the turbulent wake of a heated cylinder. Velocity measurements were made by means of hot-wire anemometry, whereas the temperature measurements were made using cold-wire thermometry.

The experiments were designed to measure both the turbulent scalar flux ($\langle u_i \theta \rangle$, where u_i is the velocity fluctuation and θ is the scalar fluctuation), and the turbulent (hydrodynamic) Reynolds stress ($\langle u_i u_j \rangle$). Furthermore, the distribution of the turbulent Prandtl number was calculated upon completion of the measurements. The latter results will be of significant benefit to numerical simulations of turbulent heat transfer. These simulations almost universally assume the turbulent Prandtl number to be equal to one.

Lastly, measurements of both the longitudinal and transverse heat flux spectra – quantities rarely measured but of significant interest to the modeling community (e.g., Bos *et al.*, 2005) – were made. Consequently, results of this work should be of interest to the engineering community that numerically simulates the turbulent transport of mass and heat.

In summary, the objectives of this thesis were to (i) obtain the technical skills to make measurements in turbulent flows, (ii) validate the preliminary measurements with relevant work, (iii) calculate the turbulent Prandtl number, and (iv) calculate the longitudinal and transverse heat flux co-spectra $E_{u\theta}$ and $E_{v\theta}$.

1.3 Thesis Overview

This thesis is divided into five chapters. Chapter 2 describes the experimental setup and measurement techniques, which include the wind tunnel, the heated cylinder, the measurement instruments, the calibration procedures, and the data acquisition and analysis. Then Chapter 3 validates individually the velocity and temperature fields. Chapter 4 shows the results obtained from the simultaneous velocity-temperature measurements. Finally, Chapter 5 gives the conclusions of this work as well as suggestions for future work.

Chapter 2

Experimental Setup and Measurement Techniques

2.1 Wind tunnel

The experiments were made in the wind tunnel located in the Aerodynamics Laboratory of McGill University. The wind tunnel's test section is 0.853 m high x 1.22 m wide with a low-turbulence intensity (0.5%). It is of suction type with a 9-to-1 contraction area ratio that follows a fifth degree polynomial contraction profile. The test section is 9 feet long and beveled corners slowly decrease in length in the downstream direction (thus increasing the cross-sectional area) to maintain a zero pressure gradient flow (and hence a constant free-stream velocity throughout the entire test section). The test section is followed by a small-angle diffuser and the axial fan is located downstream of it. The rotational speed of the fan is controlled electronically to within ±1 rpm, which ensures the stability of the mean flow. The experiments were conducted with a nominal mean flow velocity of 9.8 m/s.

2.2 Heated Cylinder

A 1″ diameter circular cylinder is used to generate the wake. This cylinder is placed vertically (in the z-direction) at the entrance of the test section. The cylinder is then heated, thus creating a heated wake.

The cylinder is made of a 1″ outer diameter aluminum pipe with $\frac{5}{64}$″ wall thickness. The cylinder is 33″ long, spanning the entire height of the tunnel's test section. Inside the cylinder there is: an electric heater of one kilowatt power with an external diameter of ¼″; a series of concentric thermal fins (25 mm in length) that fill the gap between the electric heater and the pipe. There are end supports that fix the cylinder to the walls of the test section. Heater wires at each end of the cylinder are connected to the power supply. 91% of the cylinder's length is heated using a variable AC power supply (set at 130 VAC). The cylinder can produce a maximum mean temperature rise of approximately 0.9 °C at 53 diameters downstream (x/D = 53) of it given a free-stream velocity of 9.8 m/s. Figure 2.1 shows a schematic of the experimental setup in the test section. A constant free-stream velocity (U_∞) flows past the cylinder. The coordinate axes are located at the center of the cylinder. The sensors are placed 53 diameters (x/D = 53) away from the cylinder's centre and are attached to a traversing mechanism that moves in the transverse (y) direction.

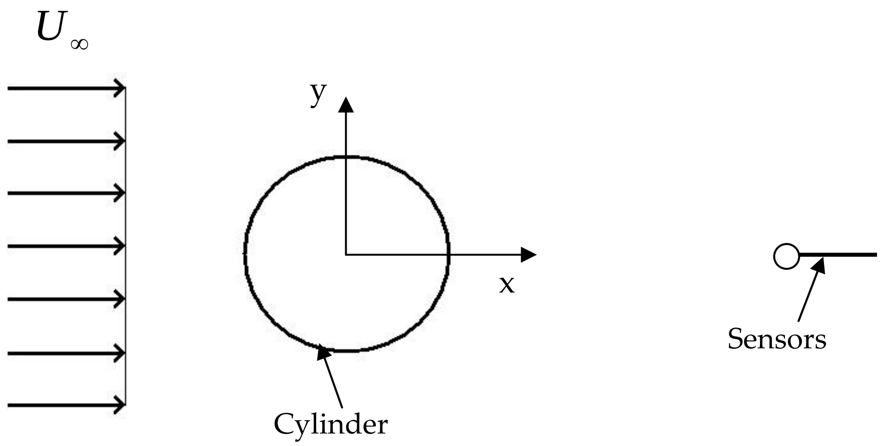

Figure 2.1: Schematic of the experimental setup in the test section

2.3 Measurement Instruments

For velocity measurements, Hot-Wire Anemometry (HWA) is used. For these measurements, the sensors are two 3μm diameter tungsten wires (with copper coating) mounted on a TSI 1241 (X-configuration probe). The wires are separated by 1 mm. Nitric acid is used to etch away the copper coating thus revealing the sensing portion of the wire. The resistance of these sensors is around 5 Ω, and the length-to-diameter ratio is on the order of 200. The constant-temperature anemometer is an IFA-300 model made by TSI with two channels.

For temperature measurements on the other hand, Cold-Wire Thermometry (CWT) operating at constant current is used. The constant-current anemometer was built at Université Laval. The sensor is a platinum wire with a diameter of 0.625μm , 0.5 mm long, mounted on a TSI 1210 single-wire probe. The resistance of cold-wires is around 150 Ω, with a length-to-diameter ratio on the order of 800.

For simultaneous velocity-temperature measurements, the X-wire probe, which measures the velocity field, is mounted beside the temperature wire (T-wire) probe. The separation distance from the T-wire to the nearest hot-wire is 1 mm. Also, the T-wire is placed 0.25 mm upstream from the centre of the X-wires. The separation should not be less than 1 mm to prevent contamination of the temperature measurements due from the hot wake of the X-wires. If the separation is much more than 1 mm, the measurements of velocity and temperature will occur at different locations across the wake. Figure 2.2 shows the arrangement of these wires.

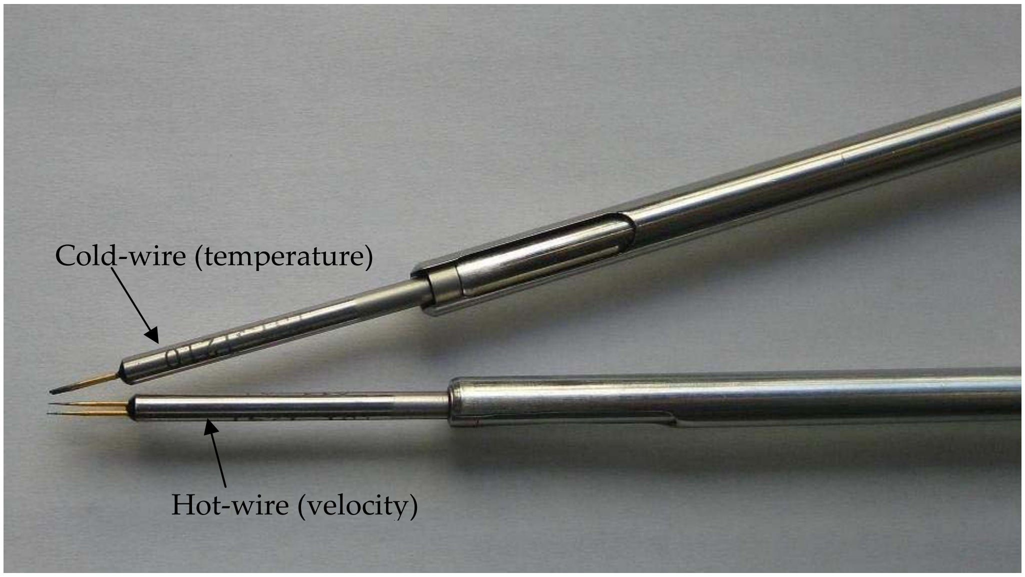

Figure 2.2: Velocity and temperature probe arrangement

2.4 Calibration Procedures

Each type of wire (cold-wire or hot-wire) requires a different calibration procedure because they rely on different physical principles to make the measurements.

2.4.1 Cold-Wire Calibration

The first step in calibrating a cold-wire is setting the current of the constant-current anemometer. If the current is too high, the wire becomes too hot and starts sensing velocity fluctuations; if it is too low, the signal-to-noise ratio will be too low. The current is selected based on the diameter of the wire. For a 0.625 μm diameter wire, the recommended current is 0.1 mA (Lemay, private communication).

The cold-wires are calibrated in a heated circular laminar jet. The jet's velocity is set to a constant value, as close as possible to the mean velocity of the experiment. The air passing through the calibration jet is heated using three 120 W electric heaters that are attached to the outside of a 2″ copper pipe connected to the calibration jet's air supply. The temperature of the jet is measured with an accuracy of ± 0.1°C using a type-E thermocouple connected to a digital display.

Once the jet is heated to a temperature above that of the ambient one (around 40°C), it is allowed to cool down by turning off the electric heaters. After a certain time, the jet's temperature decreases monotonically, which denotes the beginning of the calibration. Fourteen to seventeen points are taken at equal intervals of 0.5°C. The cold-wire thermometer output varies linearly with temperature: $T = C \times E + D$, where C and D are calibration constants determined by a least-squares fit to the calibration data. Figure 2.3 shows a typical calibration curve.

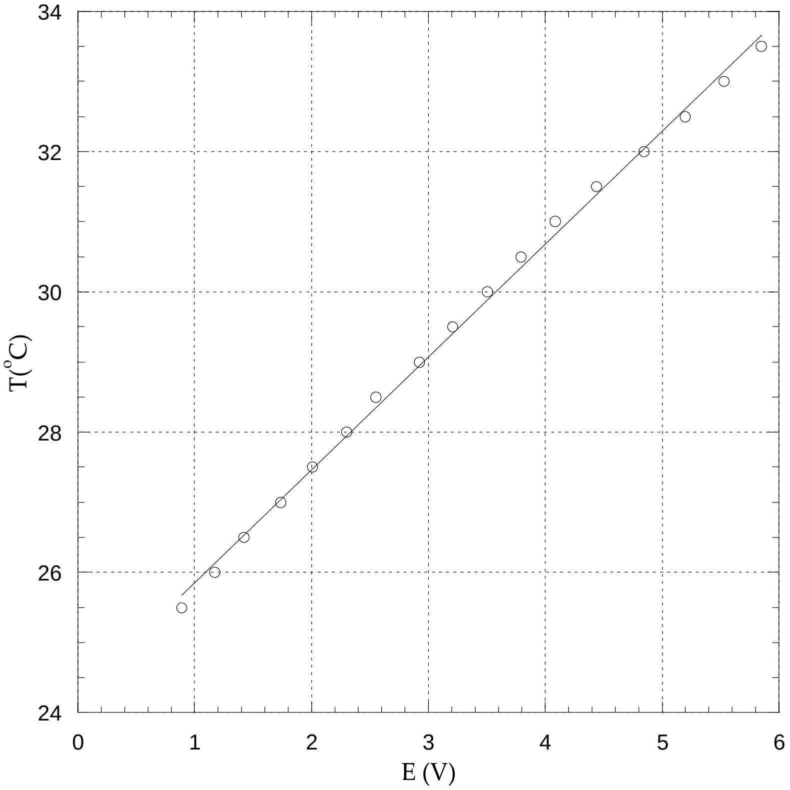

Figure 2.3: Typical temperature calibration curve

The cold-wire has a natural (thermal) frequency called the cut-off frequency (f_c). If f_c is significantly less than the Kolmogorov frequency (the highest frequency in a turbulent flow), there will be experimental error in the form of reduced temporal resolution. This error affects the small scales in the temperature field. Therefore, to improve the small-scale measurements for cold-wire thermometry, a compensation method is employed.

To do so, the time constant of the wire ($\tau_w = \dfrac{1}{2\pi f_c}$) is measured using the current injection technique proposed by Lemay and Benaïssa (2001). This technique involves injecting a square wave current through the wire. As the wire cools by forced convection, the time constant can be determined.

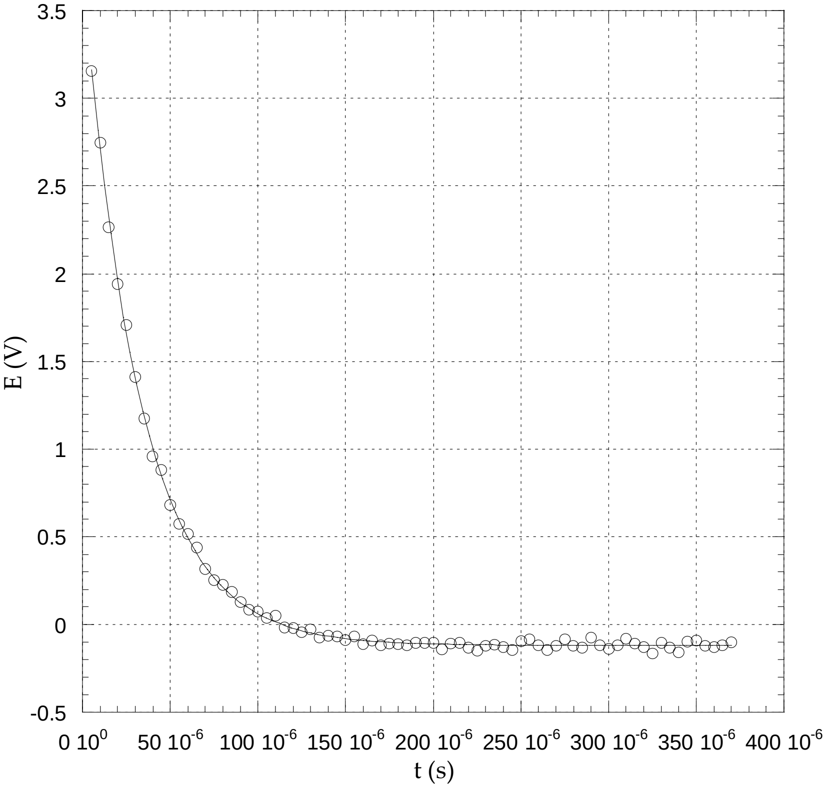

Figure 2.4: Cold-wire temporal response to the current injection technique

The following equation is proposed by Lemay and Benaïssa (2001) to model the output of the CWT in response to the current injection:

$$E = Ae^{-t/\tau_e} + Be^{-t/\tau_w} + C$$

With a least-square fit to the data (plotted in figure 2.4), the constants A, B, C, and τ_w can be found. τ_e is the time constant of the electronics; herein, $\tau_e = 3\mu\text{s}$. Therefore, f_c is found using $f_c \equiv 1/(2\pi\tau_w))$.

The compensation procedure consists of multiplying the Fourier transform of the original signal by the filter function, $H_f(f)$. The compensated signal is then obtained by taking the inverse Fourier transform of this product; the filter function used is the one put forth in Lemay and Benaïssa (2001):

$$\theta(t)_{compensated} = F^{-1}\{H_f(f)\Theta(f)_{uncompensated}\},$$

where $H_f(f)$, the filter function, is defined as:

$$H_f(f) = |H_f(f)| e^{-j\phi(f)},$$

where $|H_f(f)| = \sqrt{\dfrac{1+(f/f_c)^2}{1+(f/f_c^{'})^2}}$ is the filter gain and $\phi(f) = -\tan^{-1}\left(\dfrac{f}{f_c}\right)$ is the phase. Figure 2.5 shows the compensated and uncompensated spectra at the centerline.

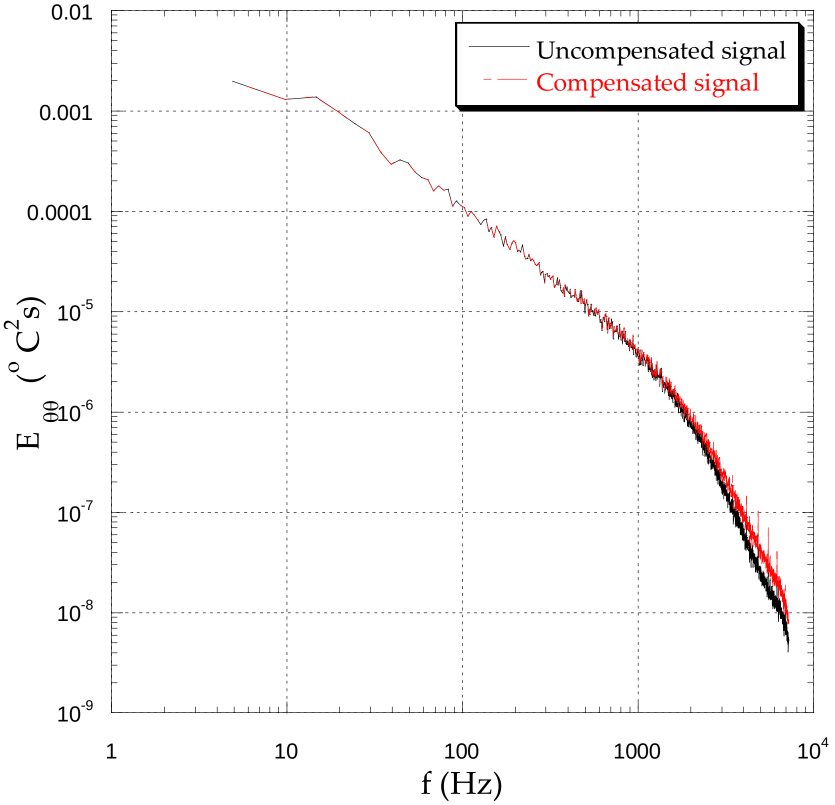

Figure 2.5: Compensated and uncompensated signal

2.4.2 Hot-Wire Calibration

Hot-wires operate at a temperature far above the ambient temperature. Hence, before performing any calibration, the material properties of the wire need to be stabilized. To do so, newly made hot-wires are operated for at least 24 hours, allowing the material properties to reach a steady-state. This procedure is called "aging" or "burning" of the hot-wires. Note that since cold-wires operate at ambient temperature, aging is not necessary.

The calibration procedure for hot-wires is more complex because the anemometer response to flow velocities is non-linear. The relationship between velocity and voltage is predicted by a modified King's Law ($E^2 = A + B \cdot U^n$), which can be derived using a forced convection heat transfer analysis of a heated cylinder. This relationship is applicable to isothermal flows, which is not the case for these experiments.

To account for the temperature fluctuations, Lienhard (1988) proposed corrections to A and B based on heat transfer principles and on the empirical effect of temperature on fluid properties:

$$A = \overline{A}\left(T_{w,a} - T_\infty\right),$$

$$B = \overline{B}\left(\frac{T_\infty + T_{w,b}}{2}\right)^{0.84}\left(T_{w,b} - T_\infty\right),$$

where T_∞ is the (varying) flow temperature and $\overline{A}$, $\overline{B}$, $T_{w,a}$, and $T_{w,b}$ are determined by calibration. $T_{w,a}$ and $T_{w,b}$ are representative of the operating temperature of the hot-wires.

The calibration procedure involves varying the jet velocity while maintaining different (constant) jet temperatures. To do so, the electric heaters are set to a certain power and allowed to reach steady-state. The velocity range is from 5 m/s to 18m/s, which corresponds to a velocity range of approximately plus or minus four standard deviations from the mean velocity of the experiment. The variation of the jet temperature for one King's Law calibration is at most ±0.8 °C. Figure 2.6 shows an example of this calibration for one of the channels (corresponding to one of the wires) of the X-wire.

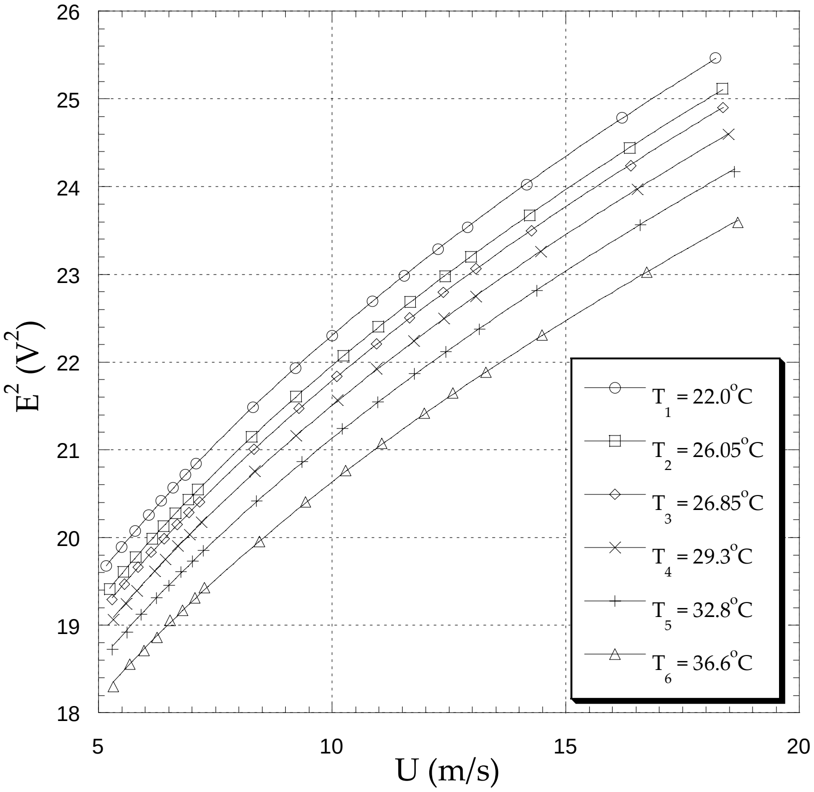

Figure 2.6: Typical calibration curves for a channel of an X-wire

King's Law is least-squares fit to each of the six velocity curves. It is then refit using an average value of the exponent n, which is approximately temperature independent. Having now found the constants A and B for each free-stream temperature, $\overline{A}$, $\overline{B}$, $T_{w,a}$, and $T_{w,b}$ are determined from the two equations listed above by least-squares fit.

To determine the u and v components of velocity, the effective angle (θ_{eff}) of each wire must be obtained by means of a yaw calibration. This calibration is done using the effective angle method described by Browne *et al.* (1989). The X-wire is calibrated using 9 different yaw angles ranging from -24 ° to 24 ° in increments of 6 ° at ambient temperature (because θ_{eff} is independent of temperature). The two hot-wires are cooled by both cross- and parallel-flow since they are not perpendicular to the flow. Browne *et al.* (1989) suggest that the ratio of the two cooling modes (k) is set constant (and independent of the orientation of the wire with respect to the flow) with a value of $(0.03)^{1/2}$. The results found for each yaw angle are then averaged giving the effective angle. Table 2.1 shows the calibration constants for the two channels of the X-wire.

Anemometer Channel	1	2
n	0.44464	0.44529
$\overline{A}\times 10^{4}$	3.4425	3.9562
$\overline{B}\times 10^{2}$	2.5490	2.5272
$T_{w,a}$	518.42	490.72
$T_{w,b}$	441.47	432.2
θ_{eff}	41.634	46.503

Table 2.1: Typical X-wire calibration constants

Note that the frequency response for hot-wires is faster than that of cold-wires due to the nature of the constant-temperature anemometry system. In the CTA manual, the frequency response of the hot-wire is stated to be 260 kHz for a 3.8 μm diameter and a flow velocity of 100 m/s. Since the maximum frequency encountered in the present flow is 10 kHz, the temporal resolution of the hot-wires is a non-issue.

2.5 Data Acquisition and Analysis

The output signals from both the CTA and the CWT are connected to a Kron-Hite model 3384 band-pass filter (for low- and high-pass filtering). They are then connected to a National Instrument PCI-6036 16-bit DAQ board. The DAQ board is controlled using LabVIEW 7.0. The probes are moved across the wake of the cylinder using a traversing mechanism that is controlled using LabVIEW. The high-pass filter is set to 0.1 Hz for all three channels (two channels are for the X-wire and one is for the cold-wire) and the low-pass filter is set to the maximum frequency of the flow at the centerline (10.7 kHz for the two X-wire channels and 7.2 kHz for the T-wire). These frequencies are approximately the Kolmogorov frequency for the two fields. They are estimated using a real-time spectrum analyzer, which is created by a Virtual Instrument controlled by LabVIEW.

An oscilloscope is used to monitor the signal from each channel and to determine the voltage span over which the data should be acquired.

Velocity and temperature measurements are assumed to be taken simultaneously even though the DAQ has an inter-channel delay of 5 μs. This assumption is valid because the time lag is only 0.04 % of the smallest Kolmogorov time scale.

For large-scale statistics, the values need to be statistically independent from one another; hence a sampling frequency on the order of the integral time scale is necessary. Therefore, the sampling frequency was set to 400 Hz with 10 blocks of 4096 samples each (for a total of 40960 data points). For spectral data, one must sample at twice the low-pass frequency, in accordance with the Nyquist criterion. Therefore, the sampling frequency was set to 21.4 kHz, with 100 blocks of 4096 samples.

The data is then processed using a computer code (written in FORTRAN 90) that converts the acquired data (voltages) to physical quantities (i.e., velocity or temperature), then performs various statistical analyses of the results.

Chapter 3

Flow Validation and the Individual Velocity and Scalar Fields

In this chapter, the velocity and scalar fields will be independently presented. The results from these measurements will be validated with theoretical predictions and previous experimental results.

3.1 Velocity Field

3.1.1 Mean and RMS Profiles of the Velocity Field

In turbulence, instantaneous measurements of quantities, such as velocity and temperature, are typically decomposed into the mean and fluctuations about the mean. This is called the Reynolds decomposition. For example, $U = \langle U \rangle + u$, where the instantaneous velocity U is decomposed into the sum of $\langle U \rangle$, the mean velocity, and u, the velocity fluctuation.

Figure 3.1 shows the transverse profile of the mean longitudinal velocity. The profile is symmetric and the velocity defect ($\langle U \rangle - U_\infty$) is Gaussian, as predicted theoretically (Tennekes and Lumley, 1972). The profile is therefore described by $< U >= A - Be^{\frac{-(y-y_o)^2}{2\sigma^2}}$, where $A = U_\infty$. At x/D = 53, the half-width ($h = \sigma\sqrt{2\ln 2}$, where σ is the standard deviation) is 2.0 diameters at the present Reynolds number of $\mathrm{Re}_D = \frac{U_\infty D}{\nu} = 15\,594$. This value falls in between the values found by Matsumura and Antonia (1993) and Kang and Meneveau (2001) when using the relationship $\frac{h_1}{h_2} = \left(\frac{(x/D)_1}{(x/D)_2}\right)^{1/2}$ to extrapolate the half-widths to the comparable downstream distance (Tennekes and Lumley, 1972). These two experiments were done at different downstream positions than the present one. Therefore, Matsumura and Antonia (1993) have a half-width of 1.7 diameters for $\mathrm{Re}_D = 5\,830$ and Kang and Meneveau (2001) have a half-width of 2.4 diameters for $\mathrm{Re}_D = 57\,960$. Furthermore, Beaulac (2003), who employed the same experimental set-up as used in this thesis, found a half-width of 2.4 diameters for slightly higher Reynolds number ($\mathrm{Re}_D = 16\,200$) and defect velocity of 1.4 at the same downstream distance (x/D = 53). (Note that the present defect velocity is 1.2.)

Moreover, the centreline velocity to free-stream velocity ratio of $\frac{U_c}{U_\infty} = \frac{8.65\mathrm{m/s}}{9.8\mathrm{m/s}} = 0.883$ is closest to the values found by Matsumura and Antonia (1993) (0.888 for x/D = 20 and 0.905 for x/D = 10 and 40) and Beaulac (2003) (0.86 for x/D = 53).

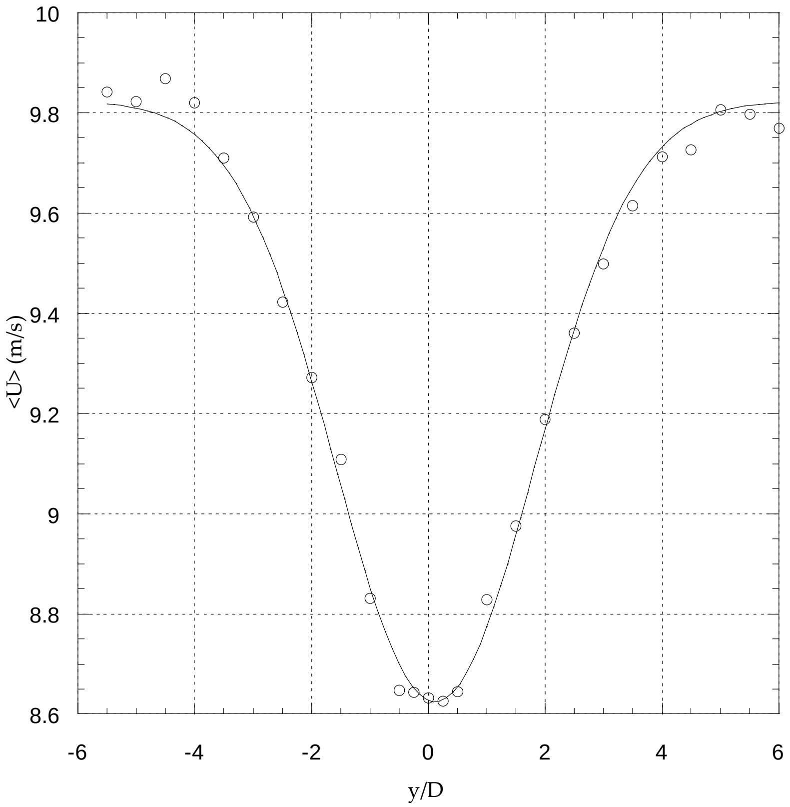

Figure 3.1: Mean Velocity Profile

Figure 3.2 shows the RMS (root-mean-square) profile of the velocity fluctuations for both velocity components (longitudinal and transverse). The highest fluctuations fall around the centre of the wake. This is consistent with previous measurements, including those of Matsumura and Antonia (1993) and Beaulac (2003).

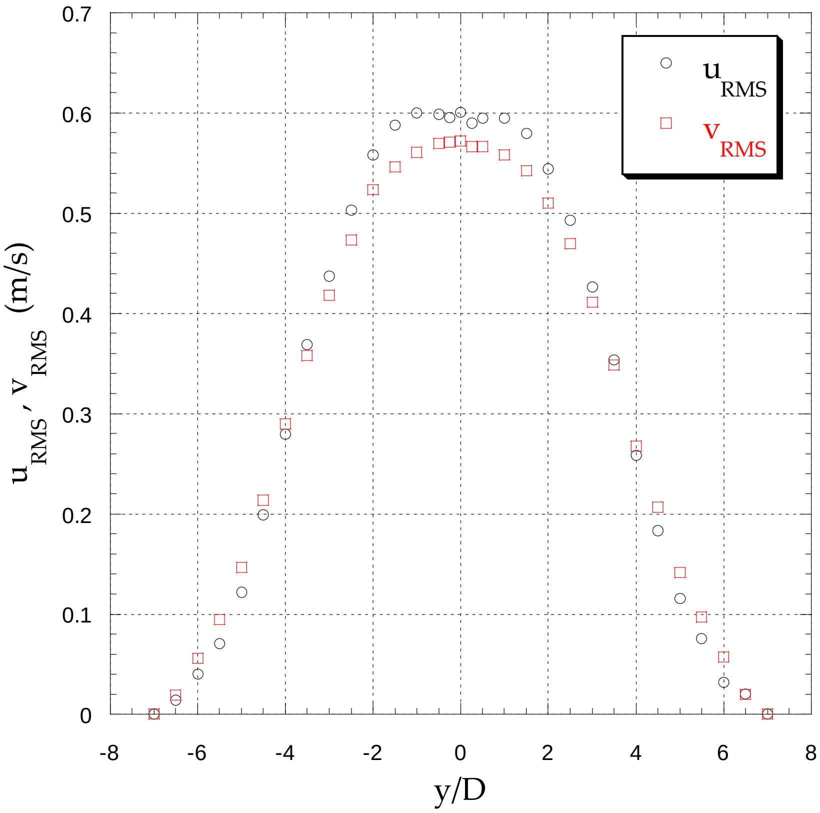

Figure 3.2: RMS profile for velocity fluctuations

Given the large aspect ratio of the cylinder (L/D = 33), the velocity field is herein assumed to be two-dimensional. This assumption was verified by Beaulac (2003), where a series of measurements were taken at different axial positions. The results from these measurements confirmed that the mean velocity profile and the RMS velocity profile, as well as the power spectral density of u, were not affected by the axial position. $(0 \le z/D \le -3.5)$

3.1.2 Power Spectral Density of the Velocity Field

The power spectral density (or power spectrum) of u is shown in figure 3.3. The power spectrum characterizes the distribution of a given quantity over the range of eddy sizes, from the largest (integral scale) eddies, to the smallest (Kolmogorov scale) eddies. Figure 3.3 plots the power spectral density of u at the centreline. It indicates that the majority of the contributions to the turbulent kinetic energy come from the lowest frequencies, which correspond to the largest eddies.

In addition, the background noise spectrum (measured with the cylinder removed from the tunnel) is shown to compare it with the turbulent signal. The signal to noise ratio is high, as desired.

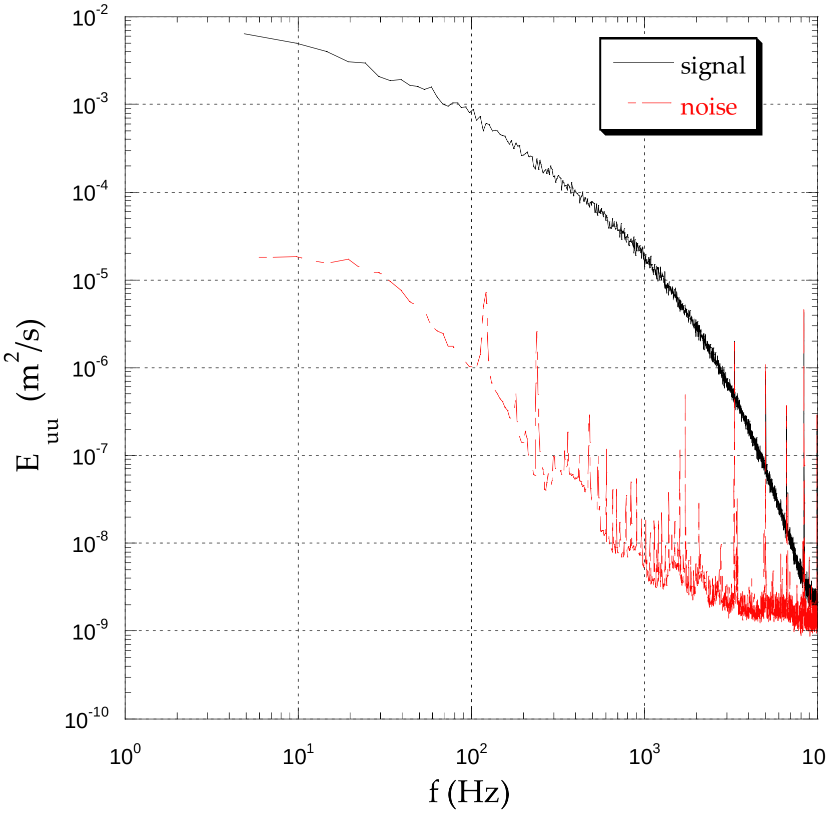

Figure 3.3: Power spectrum of the turbulent kinetic energy and the associated noise spectrum

3.1.3 Turbulent Reynolds Stress

An important parameter in the study of turbulence is the turbulent Reynolds stress, $\langle uv \rangle$. It is defined as the mean of the product of the longitudinal and transverse velocity fluctuations. This quantity would not exist if the flow were laminar and it quantifies the average momentum transfer by the turbulent eddies. Figure 3.4 plots the turbulent Reynolds stress distribution across the wake. Due to the underlying symmetries of the flow, the profile must be antisymmetric. This is confirmed in figure 3.4.

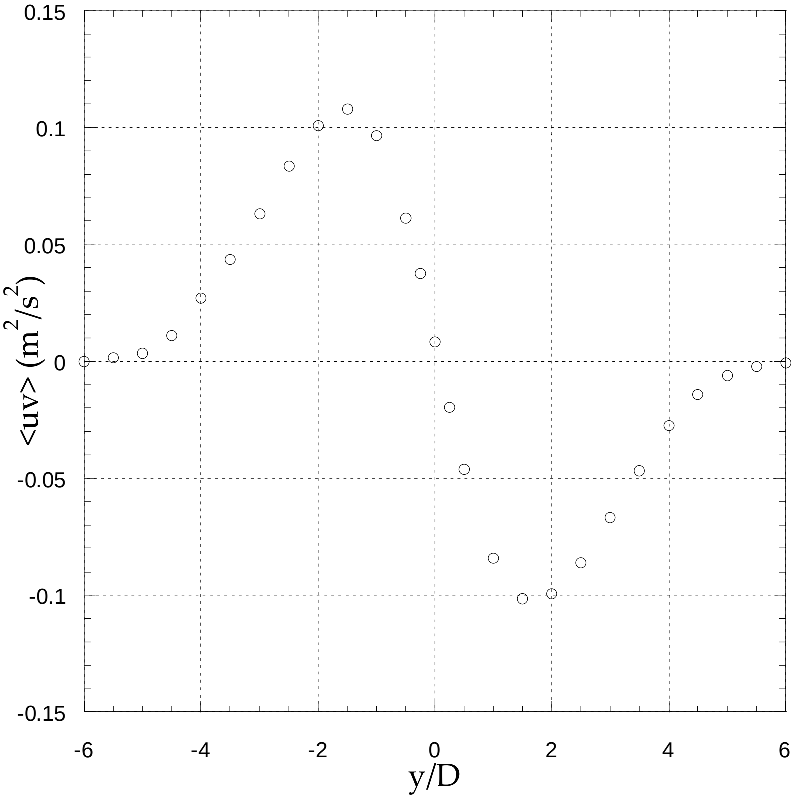

Figure 3.4: Turbulent Reynolds stress distribution

The non-dimensional form of the turbulent Reynolds stress is described by the correlation coefficient: $\rho_{uv} = \dfrac{\langle uv \rangle}{u_{RMS} v_{RMS}}$. It is zero at the centreline, as required by the symmetry of the flow. The magnitude of the peak values fall between 0.3 and 0.4, which is typical of turbulent shear flows (e.g., Pope, 2000). Outside the wake, ρ_{uv} , returns to zero, as expected.

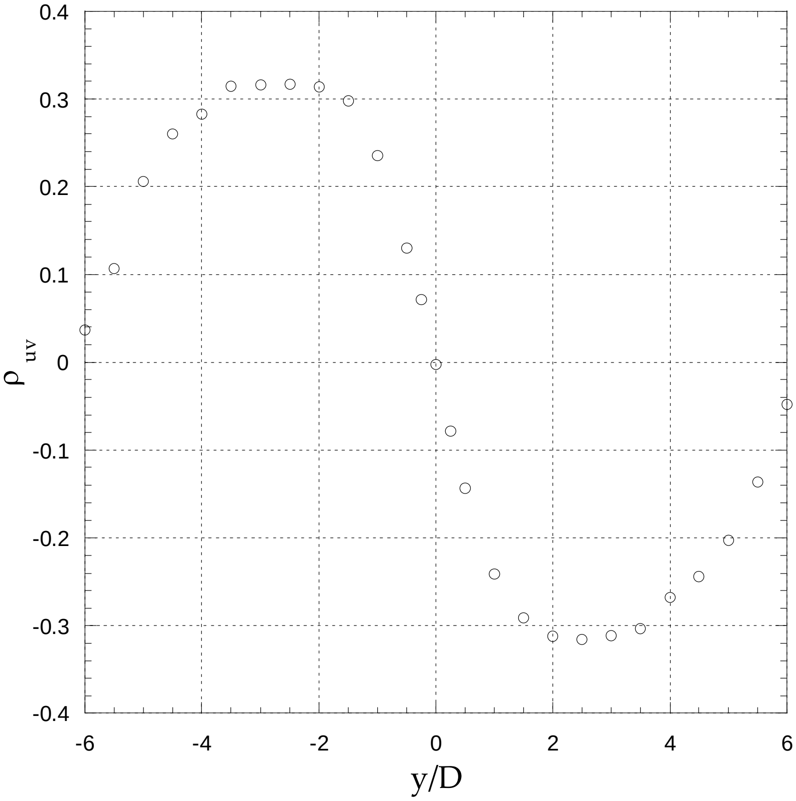

Figure 3.5: Correlation coefficient distribution

Figure 3.6 and 3.7 plot the co-spectra of the turbulent Reynolds stress at y/D = 0 and y/D = -2, respectively. At the large scales, the turbulent Reynolds stress (at y/D = 0) is on the order of magnitude of $10^{-4}(m^2/s^2)/Hz$. On the other hand, at y/D = -2, the value is on the order of magnitude of $10^{-3}(m^2/s^2)/Hz$. The mean momentum transfer is higher at y/D = -2 where the transverse velocity gradient $\left(\frac{\partial < U >}{\partial y}\right)$ is high, whereas at the centreline, the transverse velocity gradient is zero. This correlation between Reynolds stresses and mean velocity gradients is predicted by simple modelling of turbulent flows (Tennekes and Lumley, 1972; Pope, 2000).

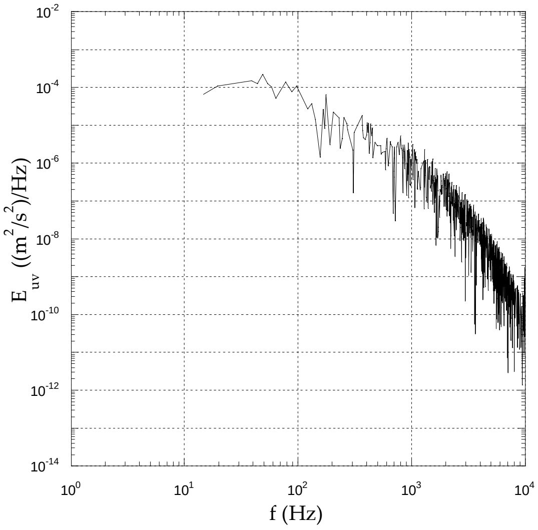

Figure 3.6: Reynolds stress co-spectrum at y/D = 0

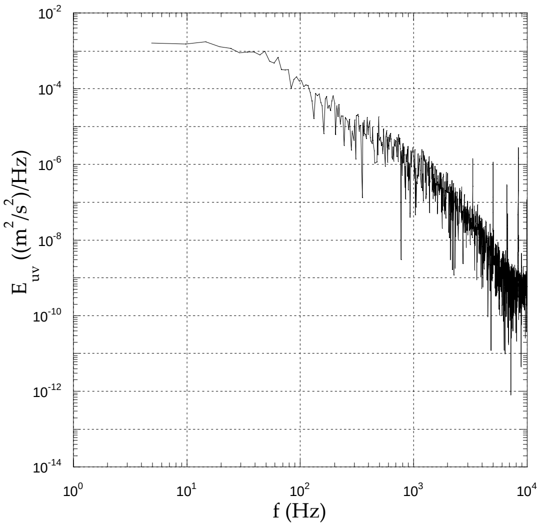

Figure 3.7: Reynolds stress co-spectrum at y/D = -2

3.2 Scalar Field

3.2.1 Mean and RMS Profiles of the Scalar Field

The mean temperature excess ($\langle T \rangle - T_\infty$) profile is plotted in figure 3.8. It assumes a Gaussian profile, similar to the velocity defect profile and as theoretically predicted, (Pope, 2000). The mean temperature excess is measured (instead of $\langle T \rangle$) to eliminate the effects of drift in ambient room temperature during the experiment. The half-width of the mean temperature excess profile is slightly larger than the half-width of the mean velocity profile with a value of 2.87 diameters. This is consistent with results from Rehab *et al.* (2001) who took measurements in the wake of a heated cylinder in a water tunnel, as well as those of Beaulac (2003).

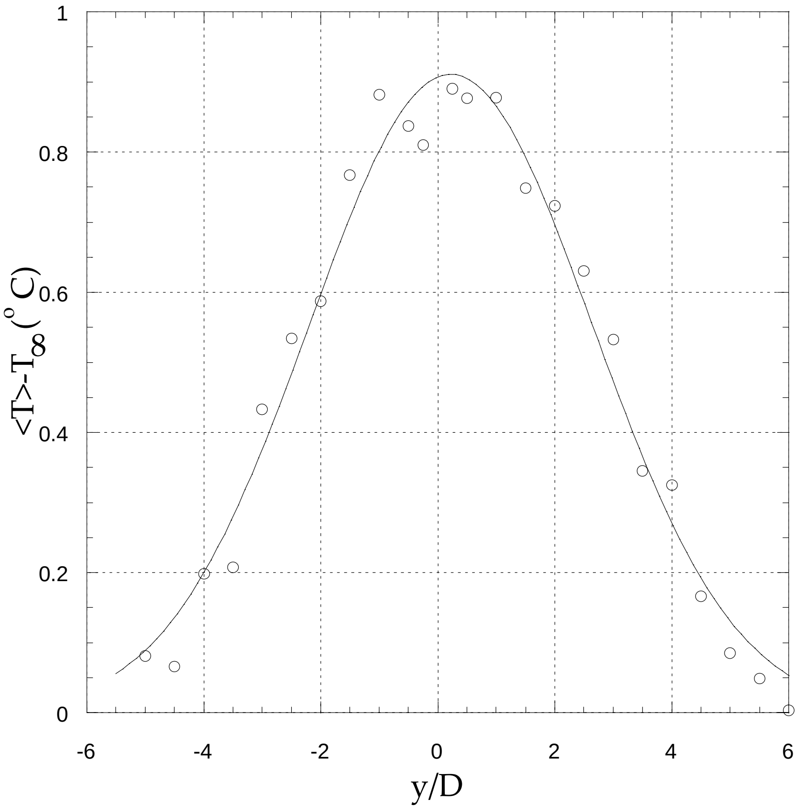

Figure 3.8: Mean temperature excess profile

Figure 3.9 shows the RMS profile of the temperature fluctuations. The profile is seen to be double-peaked, unlike that of the RMS velocity profiles, thus indicating (i) the dynamics of the two fields are not identical, and (ii) a constant unity turbulent Prandtl number assumptions may be an over-simplification. It is, however, consistent with previous measurements, including those of Matsumura and Antonia (1993) and Beaulac (2003).

Lastly, the scalar field was also found to be two-dimensional by Beaulac (2003), once again, by measuring RMS profiles and power spectral densities at different axial positions.

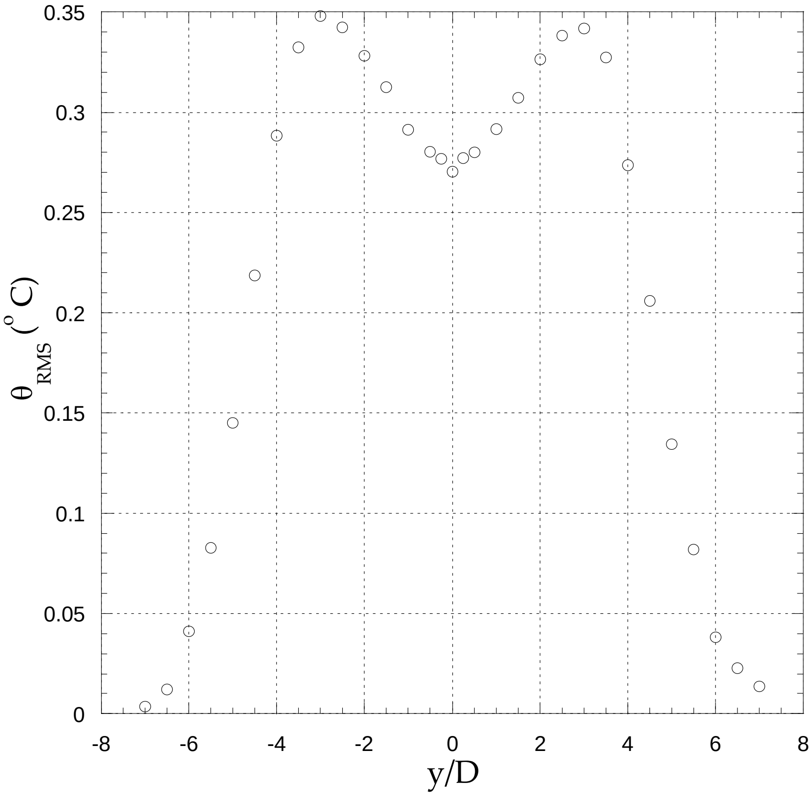

Figure 3.9: RMS profile for the temperature fluctuations

3.2.2 Power Spectral Density for the Scalar Field

Figure 3.10 shows the power spectral densities (of both the signal and the noise) of the scalar field. The background noise is measured within the turbulent wake when the cylinder is not heated. The noise consists of electronic noise, noise caused by ambient temperature fluctuations, and the temperature wire's sensitivity to the velocity fluctuations. Electronic noise is the cause of the spikes at frequencies of 60 Hz and its harmonics. Since the noise spectrum is many decades lower than the signal spectrum, the measured noise is not a significant factor in the results. Finally, it can be observed that the majority of the contributions to the scalar variance come from the large (low-frequency) scales.

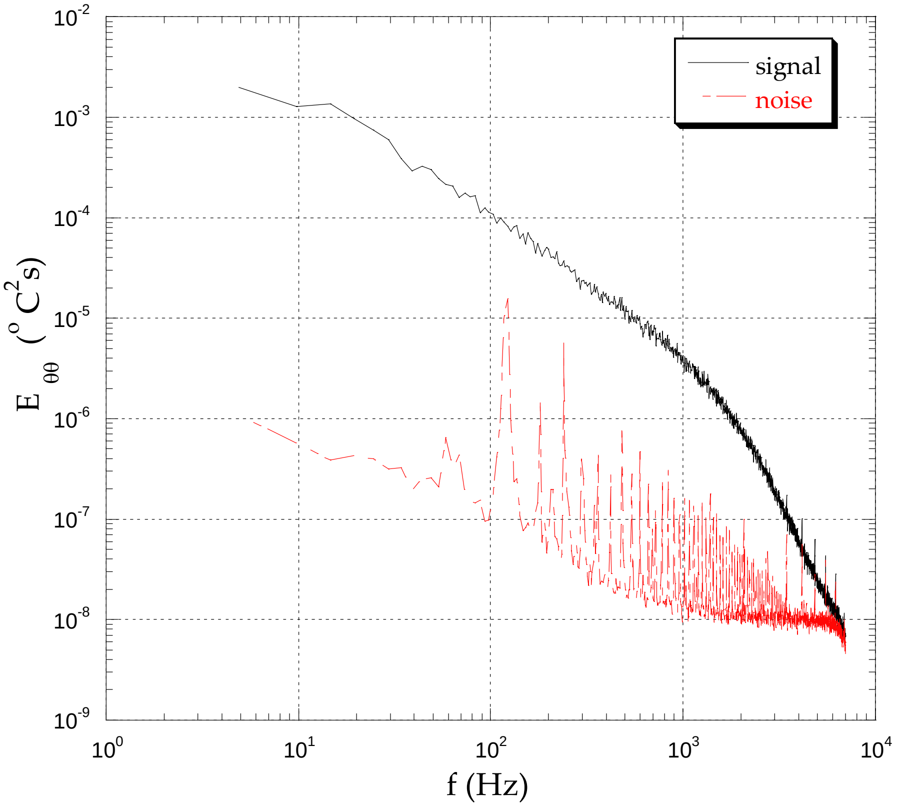

Figure 3.10: Power spectrum of the scalar variance and the associated noise spectrum

Chapter 4

Simultaneous Velocity-Temperature Measurements

In this chapter, *simultaneous* velocity-temperature measurements will be presented. These include the turbulent heat flux, the turbulent heat flux co-spectra, and the turbulent Prandtl number distribution.

4.1 Turbulent Heat Fluxes

4.1.1 Longitudinal Turbulent Heat Flux

The longitudinal turbulent heat flux, $\langle u\theta \rangle$, is the mean of the longitudinal velocity and temperature fluctuations. It describes how the velocity fluctuations in the longitudinal direction mix the scalar. Figure 4.1 plots the transverse profile of the longitudinal turbulent heat flux. The profile is symmetric since both U and T are symmetric across the wake. The values of $\langle u\theta \rangle$ are negative because low velocities at the centre of the wake correspond to high temperatures (and vice versa at the edges of the wake).

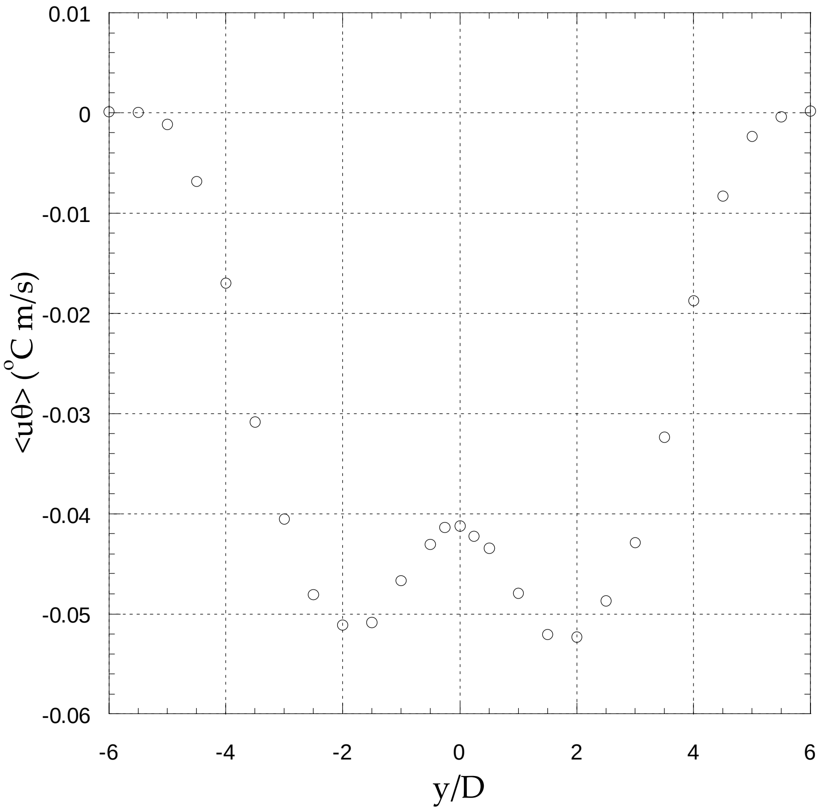

Figure 4.1: Longitudinal turbulent heat flux profile

The co-spectra of the longitudinal turbulent heat flux are shown in figures 4.2 and 4.3 at y/D = 0 and y/D = -2, respectively. A comparison of the two plots indicates that both spectra are of approximately the same magnitude (and on the order of $10^{-3}(m/s)^{\circ}C/Hz$ at large scales / small frequencies). This result is consistent with the relatively uniform values of $\langle u\theta \rangle$ across the centre of the wake.

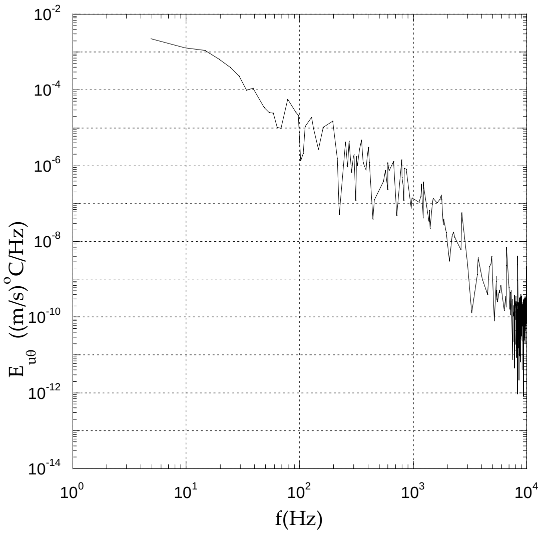

Figure 4.2: Longitudinal heat flux co-spectrum at y/D = 0

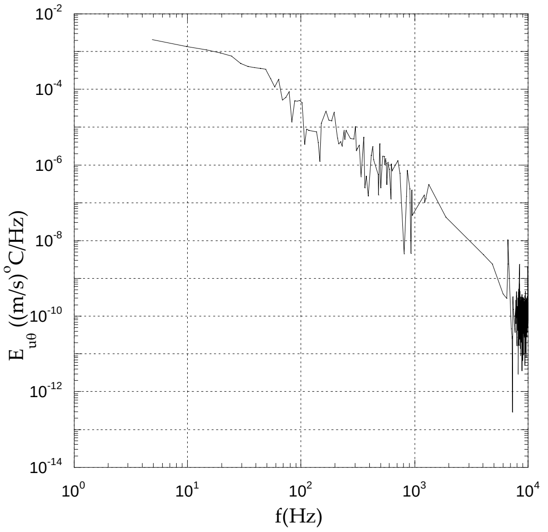

Figure 4.3: Longitudinal heat flux co-spectrum at y/D = -2

4.1.2 Transverse Turbulent Heat Flux

The transverse turbulent heat flux, $\langle v\theta \rangle$, is the mean of the transverse velocity and temperature fluctuations. It describes how the velocity fluctuations in the transverse direction mix the scalar. Figure 4.4 plots the profile of the transverse turbulent heat flux. The profile is antisymmetric since the transverse velocity is antisymmetric, and the scalar is symmetric, across the wake of the cylinder.

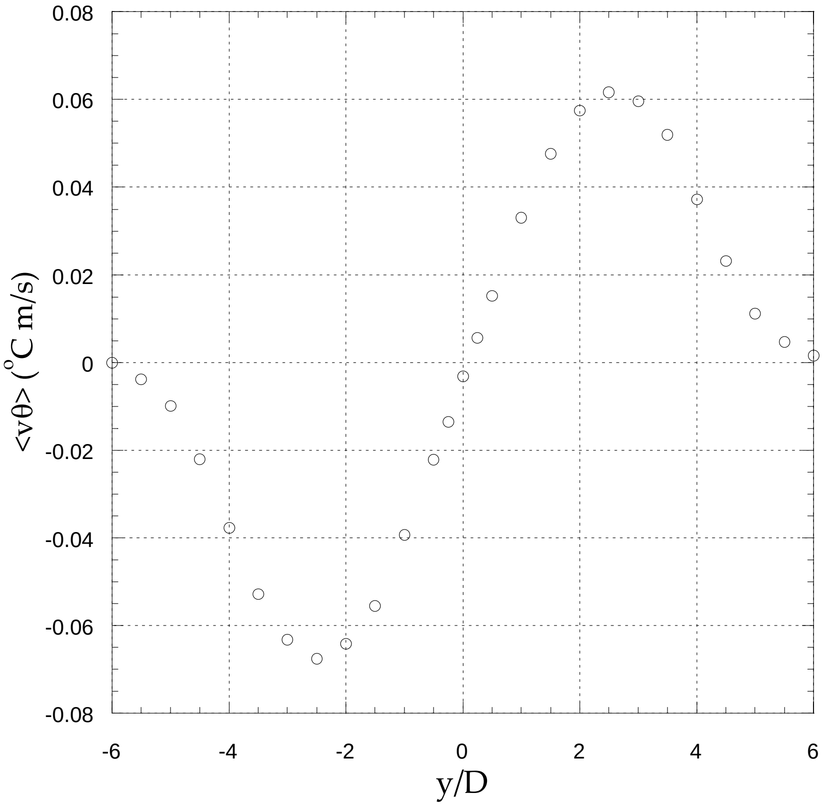

Figure 4.4: Transverse turbulent heat flux profile

The co-spectra of the longitudinal turbulent heat flux are shown in figures 4.5 and 4.6 at y/D = 0 and y/D = -2, respectively. At large scales, the transverse turbulent heat flux at y/D = 0 is on the order of magnitude of $10^{-4}(m/s)^{\circ}C/Hz)$. On the other hand, at y/D = -2, the value is on the order of magnitude of $10^{-3}(m/s)^{\circ}C/Hz)$. The conclusion that can be drawn from this difference is that the heat transfer in the transverse direction is higher away from the centreline, at the location of high temperature gradients. Such a result is consistent with the gradient transport hypothesis (Pope, 2000) which suggests that the turbulent heat flux is proportional to the local mean temperature gradient.

Looking at figure 4.6, one can observe a power-law region that is called the "inertial subrange." Herein, the mixing does not depend on the geometry of the flow (characterized by the large scales) nor on the viscous molecular effects (characterized by the small scales). The value of the power-law exponent for this co-spectrum is approximately -2.

Lumley (1967) theoretically predicted that, at high Reynolds numbers, the power-law exponent should tend to -7/3. However, few experimental results exist with which to compare this prediction. Mydlarski (2003) measured (transverse) heat flux co-spectra in homogeneous, isotropic, grid turbulence with an imposed mean temperature gradient. He also observed a value of approximately -2 for the inertial-range slope of the co-spectrum, consistent with the present results in the wake of a heated cylinder, which, I emphasize, is an *inhomogeneous* turbulent flow.

Bos and Bertoglio (2007) proposed a model for the study of the Reynolds number dependence of the scalar flux spectra in homogeneous turbulent shear flow with a uniform cross-stream scalar gradient. They found that the inertial-range scaling exponent of the cross-stream scalar flux spectrum tends to -7/3 for large Reynolds numbers, but at lower Reynolds numbers, typical of the present work and that of Mydlarski (2003), it was closer to -2.

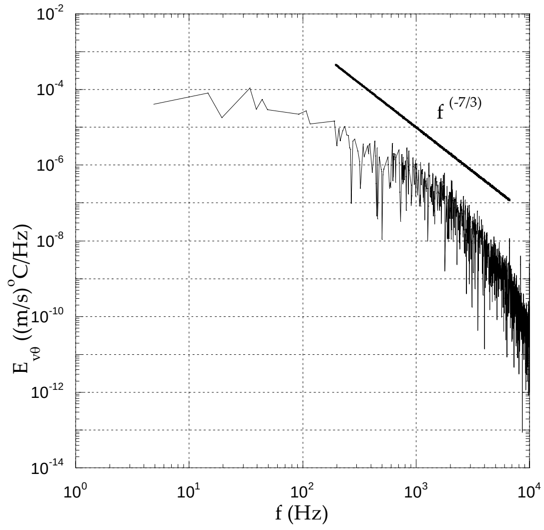

Figure 4.5: Transverse heat flux co-spectrum at y/D = 0

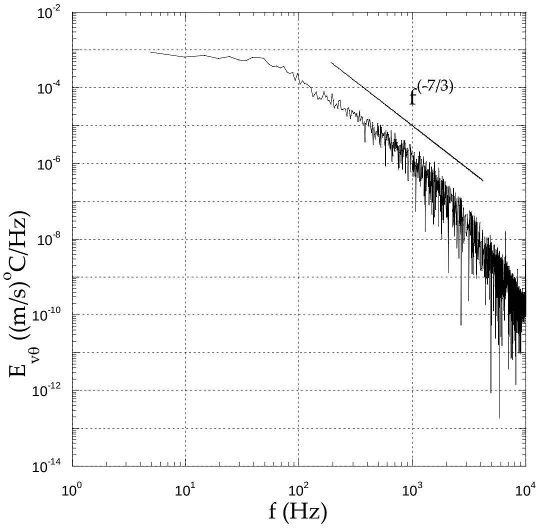

Figure 4.6: Transverse heat flux co-spectrum at y/D = -2

Comparing the longitudinal (figure 4.1) and transverse (figure 4.4) turbulent heat flux profiles, it can be seen that the maximum absolute value of the turbulent heat flux is higher for the transverse direction ($\langle v\theta \rangle = 0.07\dfrac{m^{\circ}C}{s}$) than in the longitudinal direction ($\langle u\theta \rangle = 0.052\dfrac{m^{\circ}C}{s}$). This is consistent with larger heat transfer in the transverse direction, where the temperature gradients are larger (Pope, 2000).

4.2 Turbulent Prandtl Number

As mentioned in Chapter 1, the turbulent Prandtl number, $\Pr_T \equiv \frac{\nu_T}{\gamma_T}$, is defined as the ratio of the turbulent momentum diffusivity, ν_T, (also known as the turbulent viscosity) to the turbulent thermal diffusivity, γ_T. It relates how well turbulence transports momentum compared to energy.

Turbulent diffusivities are defined by the gradient transport hypothesis (Tennekes and Lumley, 1972, and Pope, 2000). They are the coefficients of proportionality between the turbulent momentum (heat) fluxes and the local mean velocity (temperature) gradients. The gradient transport hypothesis is a turbulent analogy to the molecular transport of momentum (energy) by viscosity (thermal diffusivity) as given by the definition of a Newtonian fluid (Fourier's Law). As such, the turbulent Prandtl number can be defined as follows:

$$\Pr_T = \frac{\nu_T}{\gamma_T} = \frac{-\dfrac{<uv>}{\left(\dfrac{\partial <U>}{\partial y}\right)}}{-\dfrac{<v\theta>}{\left(\dfrac{\partial <T>}{\partial y}\right)}}$$

Figure 4.7 plots the distribution of the turbulent Prandtl number across the wake of the cylinder. As also mentioned in Chapter 1, the turbulent Prandtl number is generally assumed to be unity. The experimental results show that this assumption is not accurate. Although the turbulent Prandtl number is on the order of magnitude of one, it does vary significantly across the wake from a value of 0.8 to 1.2. At both the edges and centre of the wake, the velocity and temperature gradients are zero, which explains the outlying values of the turbulent Prandtl number. In summary, the assumption of a constant turbulent Prandtl number across the wake is clearly inadequate.

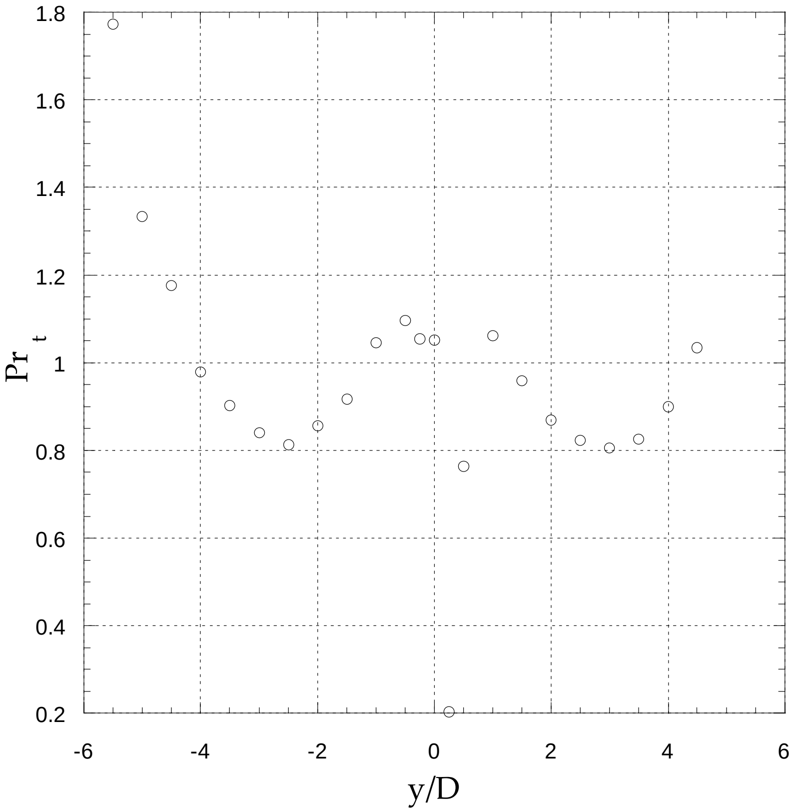

Figure 4.7: Turbulent Prandtl number distribution

Chapter 5

Conclusions

The goal of this work was to study the mixing of scalars by taking simultaneous velocity-scalar measurements in a turbulent flow. The scalar used was temperature which was considered to be passive. To achieve this goal, mixed velocity-temperature measurements were made in the turbulent wake of a heated cylinder, placed in a wind tunnel.

With the results from the mixed velocity-temperature measurements, the turbulent heat flux, which describes how velocity fluctuations mix the scalar fluctuations, was quantified. By comparing the longitudinal and transverse turbulent heat flux profile, it was shown that heat transfer in transverse direction is higher than in the longitudinal direction. Furthermore, the heat flux co-spectra confirmed that the turbulent heat flux is proportional to the local mean temperature gradient.

Furthermore, the inertial-range scaling of the transverse heat flux co-spectra was studied. Interestingly, this co-spectra exhibited inertial-range scalings similar to those observed in homogeneous, isotropic turbulence with a power-law exponent of approximately -2, even though the present flow is clearly inhomogeneous.

Finally, the turbulent Prandtl number (Pr_T) distribution across the wake was determined to verify the common assumption that the turbulent Prandtl number is equal to unity. The distribution showed that, although the turbulent Prandtl number is on the order of magnitude of one, it does vary significantly across the wake from a value of 0.8 to 1.2.

5.1 Future Work

For future research, further investigation of the turbulent heat flux co-spectra (transverse and longitudinal) is desired; especially the interest is in investigating the inertial subrange of the longitudinal turbulent heat flux co-spectra to determine the power-law exponent and compare it with both co-spectra.

Also, studying the mixed structure functions, $\left\langle (\Delta u_i(r))^n (\Delta\theta(r))^m \right\rangle$,and in particular, the heat flux structure functions $\left\langle (\Delta u_i)(\Delta\theta)^2 \right\rangle$ is of interest. (Heat flux structure functions are the real-space analogue of the (one-dimensional) co-spectra of velocity and temperature).

Danaila and Mydlarski (2001) studied the heat flux structure functions in decaying grid turbulence with an imposed temperature gradient. They compared theoretical predictions from Yaglom (1949) (called Yaglom’s equation) to their experimental data, and found that the agreement between theory and experiment was good.

Yaglom's four-thirds law predicts that for large Reynolds numbers, in the inertial-range: $\left\langle (\Delta u_i(r))(\Delta\theta(r))^2 \right\rangle = -\frac{4}{3}\langle \in_\theta \rangle r$ (where $\in_\theta$ is the rate of destruction of the scalar variance).

Therefore, verifying the theoretical predictions of Yaglom for a different kind of turbulent flow (inhomogeneous turbulence), by taking simultaneous velocity-temperature measurements in the wake of a heated cylinder, would be a beneficial way of confirming the universality of these predictions.

Finally, the sixth order structure functions, where n=2 and m=4, are also worth investigating to determine the effect of internal intermittency of a passive scalar field.

References

Beaulac, S. 2003 The Effect of the Injection Scale on Scalar Mixing in the Turbulent Wake of a Circular Cylinder. M Eng thesis, McGill University.

Bos, W. J. T. & Bertoglio, J.-P. 2007 Inertial range scaling of scalar flux spectra in uniformly sheared turbulence, *Phys. Fluids* **19**, 025104.

Bos, W. J. T., Touil, H. & Bertoglio, J.-P. 2005 Reynolds number dependency of the scalar flux spectrum in isotropic turbulence with a uniform scalar gradient, *Physics of Fluids* **17**, 125108.

Browne, L. W. B., Antonia, R. A. & Chua, L. P. 1989 Calibration of X-Probes for Turbulent Flow Measurements, *Exps. Fluids* **7**, 201-208.

Brunn, H. H. 1995 *Hot-Wire Anemometry: Principles and Signal Analysis*, Oxford University Press.

Danaila, L. & Mydlarski, L. 2001 Effect of gradient production on scalar fluctuations in decaying grid turbulence. *Phys Rev.* E **64**, 0163161-0163169.

Kang, H. S. & Meneveau, C. 2001 Passive scalar anisotropy in a heated turbulent wake: new observations and implications for large-eddy simulations, *J. Fluid. Mech.* **442**, 161-170.

Kays, W. M. 1994 Turbulent Prandtl number – Where are we? *Journal of Heat Transfer* **116**, 284-295.

Lemay, J. 2007 Notice d'utilisation des anémomètres à courant constant, *Private Communication.*

Lemay, J. & Benaïssa, A. 2001 Improvement of cold-wire response for measurements of temperature dissipation, *Exps. Fluids* **31**, 347-356.

Lesieur, M. & Metais, O. 1996 New trends in Large-Eddy Simulations of turbulence, *Ann. Rev. Fluid Mech*. **28**, 45-82.

Lienhard, J. H. 1988 The Decay of Turbulence in Thermally Stratified Flow, PhD dissertation, University of California at San Diego.

Lumley, J. L. 1967 Similarity and the turbulent energy spectrum, *J. Fluid. Mech.* **10**, 855-858.

Matsumura, M. &Antonia, R. A. 1993 Momentum and heat transport in the turbulent intermediate wake of a circular cylinder, *J. Fluid. Mech.* **250**, 651-668.

Moin, P. & Mahesh, K. 1998 Direct Numerical Simulation: A tool in turbulence research, *Ann. Rev. of Fluid Mech*. **30**, 539-578.

Mydlarski, L. 2003 Mixed velocity-passive scalar statistics in high-Reynolds-number turbulence, *J. Fluid. Mech.* **475**, 173-203.

Pope, S. B. 2000 *Turbulent Flows*, Cambridge University Press.

Rehab, H., Antonia, R. A. & Djendji, L. 2001 Streamwise evolution of a high-Schmidt number passive scalar in a turbulent plane wake, *Exp. Fluids* **31**, 186-192.

Sreenivasan, K. R., Antonia, R. A. & Chambers, A. J. 1984 On the variation of the turbulent Prandtl number in shear flows, *Int. Comm. Heat Mass Transfer* **11 no 5**, 497-501.

Tennekes, H. & Lumley, J. L. 1972 *A First Course in Turbulence*. MIT Press.

Townsend, A. A. 1976 *The Structure of Turbulent Shear Flows*, 2nd edition, C. U. Cambridge, U. K.

Yaglom, A. M. 1949 On the local structure of a temperature field in a turbulent flow, *Dokl. Akad. Nauk*. SSSR **69**, 743-746.